Elastography
General Principles and Clinical Applications

Marvin M. Doyley, PhD*, Kevin J. Parker, PhD

KEYWORDS

• Elastography • Ultrasonic imaging • Ultrasonic elastography • MRI

KEY POINTS

- Like conventional medical imaging modalities, forward and the inverse problems are encountered in elastography.
- Quasistatic elastography visualizes the strain induced within tissue using either an external or internal source.
- Direct and iterative inversion schemes have been developed to make quasistatic elastograms more quantitative.
- Soft tissues display several biomechanical properties, including viscosity and nonlinearity, which may improve the diagnostic value of elastography when visualized alone or in combination with shear modulus. Elastography can characterize the nonlinear behavior of soft tissues and may be used to differentiate between benign and malignant tumors.

INTRODUCTION

Elastography visualizes differences in the biomechanical properties of normal and diseased tissues.[1–4] Elastography was developed in the late 1980s to early 1990s to improve ultrasonic imaging,[5–7] but the success of ultrasonic elastography has inspired investigators to develop analogs based on MRI[8–11] and optical coherence tomography.[12–14] This article focuses on ultrasonic techniques with a brief reference to approaches based on MRI.

The general principles of elastography can be summarized as follows: (1) perturb the tissue using a quasistatic, harmonic, or transient mechanical source; (2) measure the resulting mechanical response (displacement, strain or amplitude, and phase of vibration); and (3) infer the biomechanical properties of the underlying tissue by applying either a simplified or continuum mechanical model to the measured mechanical response.[2,15–18] This article describes (1) the general principles of quasistatic, harmonic, and transient elastography (**Fig. 1**)—the most popular approaches to elastography—and (2) the physics of elastography—the underlying equations of motion that govern the motion in each approach. Examples of clinical applications of each approach are provided.

THE PHYSICS OF ELASTOGRAPHY

Like conventional medical imaging modalities, forward and the inverse problems are encountered in elastography. The former problems are concerned with predicting the mechanical response of a material with known biomechanical properties and external boundary conditions. Understanding these problems and devising accurate theoretical models to solve them have been an effective strategy in developing and optimizing the performance of ultrasound displacement estimation methods. The latter problems are concerned with estimating biomechanical properties noninvasively using the forward model and knowledge of the mechanical response and external boundary conditions. A comprehensive review of methods developed to

Department of Electrical and Computer Engineering, University of Rochester, Hopeman Engineering Building 343, Box 270126, Rochester, NY 14627, USA
* Corresponding author.
E-mail address: m.doyley@rochester.edu

Ultrasound Clin 9 (2014) 1–11
http://dx.doi.org/10.1016/j.cult.2013.09.006
1556-858X/14/$ – see front matter Published by Elsevier Inc.

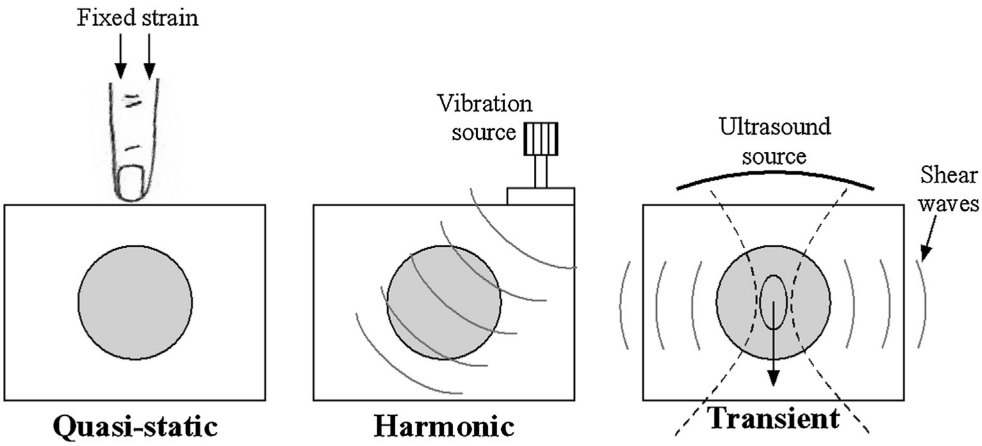

Fig. 1. Schematic representation of current approaches to elastographic imaging: quasistatic elastography (*left*), harmonic elastography (*middle*), and transient elastography (*right*).

solve inverse problems is given in the article by Doyley[19]; therefore, this section focuses only on the forward problem.

The forward elastography problem can be described by a system of partial differential equations (PDEs) given in compact form[20,21]:

$$\nabla \times [\sigma_{ij}] = \beta_i \quad \textbf{(1)}$$

where σ_{ij} is the 3-D stress tensor (ie, a vector of vectors), β_i is the deforming force, and ∇ is the del operator. Using the assumption that soft tissues exhibit linear elastic behavior, then the strain tensor (ε) maybe related to the stress tensor (σ) as follows[22]:

$$\sigma_{ij} = C_{ijkl}\varepsilon_{kl} \quad \textbf{(2)}$$

where the tensor (C) is a rank-four tensor consisting of 21 independent elastic constants.[16,20,23] Under the assumption that soft tissues exhibit isotropic mechanical behavior, however, then only 2 independent constants, λ and μ (lambda and shear modulus), are required. The relationship between stress and strain for linear isotropic elastic materials is given by:

$$\sigma_{ij} = 2\mu\varepsilon_{ij} + \lambda\delta_{ij}\Theta \quad \textbf{(3)}$$

where $\Theta = \nabla \cdot \mathbf{u} = \varepsilon_{11} + \varepsilon_{22} + \varepsilon_{33}$ is the compressibility relation, δ is the Kronecker delta, and the components of the strain tensor are defined as:

$$\varepsilon_{ij} = \frac{1}{2}\left(\frac{\partial u_i}{\partial j} + \frac{\partial u_j}{\partial x_i}\right) \quad \textbf{(4)}$$

Lamé constants (ie, λ and μ) are related to Young modulus (E) and Poisson ratio (v), as follows[20,21]:

$$\mu = \frac{E}{2(1+v)}, \quad \lambda = \frac{vE}{(1+v)(1-2v)} \quad \textbf{(5)}$$

The stress tensor is eliminated from the equilibrium equations (ie, Equation 2) using Equation 3. The strain components are then expressed in terms of displacements using Equation 4. The resulting equations (ie, the Navier-Stokes equations) are given by:

$$\nabla \cdot \mu \nabla \mathbf{u} + \nabla(\lambda+\mu)\nabla \cdot \mathbf{u} = \rho \frac{\partial^2 \mathbf{u}}{\partial t^2} \quad \textbf{(6)}$$

where ρ the is density of the material, ***u*** is the displacement vector, and t is time. For quasistatic deformations, Equation 6 reduces to:

$$\nabla \cdot \mu \nabla \mathbf{u} + \nabla(\lambda+\mu)\nabla \cdot \mathbf{u} = 0 \quad \textbf{(7)}$$

For harmonic deformations, the time-independent (steady-state) equations in the frequency domain give[10,24]:

$$\nabla \cdot \mu \nabla \mathbf{u} + \nabla(\lambda+\mu)\nabla \cdot \mathrm{u} = \rho\omega^2 \mathbf{u} \quad \textbf{(8)}$$

where ω is the angular frequency of the sinusoidal excitation. For transient deformations, the wave equation is derived by differentiating Equation 6 with respect to *x, y,* and *z,* which gives[21]:

$$\nabla^2 \Delta = \frac{1}{c_1^2}\frac{\partial^2 \Delta}{\partial t^2} \quad \textbf{(9)}$$

where $\nabla \cdot \mathbf{u} = \Delta$, and the velocity of the propagating compressional wave, c_1, is given by:

$$c_1 = \sqrt{\frac{\lambda + 2\mu}{\rho}} \quad \textbf{(10)}$$

The wave equation for the propagating shear wave is given by:

$$\nabla^2 \zeta = \frac{1}{c_2^2}\frac{\partial^2 \zeta}{\partial t^2} \quad \textbf{(11)}$$

where $\zeta = \nabla \cdot u/2$ is the rotational vector, and the shear wave velocity, c_2, is given by:

$$c_2 = \sqrt{\frac{\mu}{\rho}} \quad (12)$$

Analytical methods have been used to solve the governing equations for quasistatic, harmonic, and transient elastographic imaging methods[25–28] for simple geometries and boundary conditions. Numeric methods—namely, the finite-element method—are used, however, to solve the governing equations for all 3 approaches to elastography on irregular domains and for heterogeneous elasticity distributions.[24,29–36]

APPROACHES TO ELASTOGRAPHY

Quasistatic Elastography

Quasistatic elastography visualizes the strain induced within tissue using either an external or internal source. A small motion is induced within the tissue (typically approximately 2% of the axial dimension) with a quasistatic mechanical source. The axial component of the internal tissue displacement is measured by performing cross-correlation analysis on pre- and postdeformed radiofrequency (RF) echo frames[6,7,37] and strain is estimated by spatially differentiating the axial displacements. In quasistatic elastography, soft tissues are typically viewed as a series of 1-D springs that are arranged in a simple fashion. For this simple mechanical model, the measured strain (ε) is related to the internal stress (σ) by Hooke's law:

$$\sigma = k\varepsilon \quad (13)$$

where k is the Young modulus (or stiffness) of the tissue. No method can measure the internal stress distribution in vivo; consequently, the internal stress distribution is assumed to be constant (ie, $\sigma \approx 1$); an approximate estimate of Young modulus is computed from the reciprocal of the measured strain. The disadvantage of computing modulus elastograms in this manner is that it does not account for stress decay or stress concentration; consequently, quasistatic elastograms typically contain target-hardening artifacts,[31,35] as illustrated in **Fig. 2**.

Despite this limitation, several groups have obtained good elastograms in applications where accurate quantification of Young modulus is not essential. For example, **Fig. 3** shows the results of a case study, where quasistatic elastography was performed on a 73-year-old woman with a phyllodes tumor in the upper outer quadrant of her left breast. Phyllodes tumors are rare variants of fibroadenoma, with a rich stromal component and more cellularity. They grow quickly, developing macroscopically lobulated internal structures and may reach a large size, visibly altering the breast profile. Sonography generally shows a solid, moderately hypoechoic nodule with smooth borders and good sound transmission.[38] Inhomogenous structures may be present because of small internal fluid areas. These appearances are nonspecific, and sonography is not currently able to distinguish between benign and malignant cases, nor can it make a differential diagnosis between fibroadenoma and phyllodes tumors.

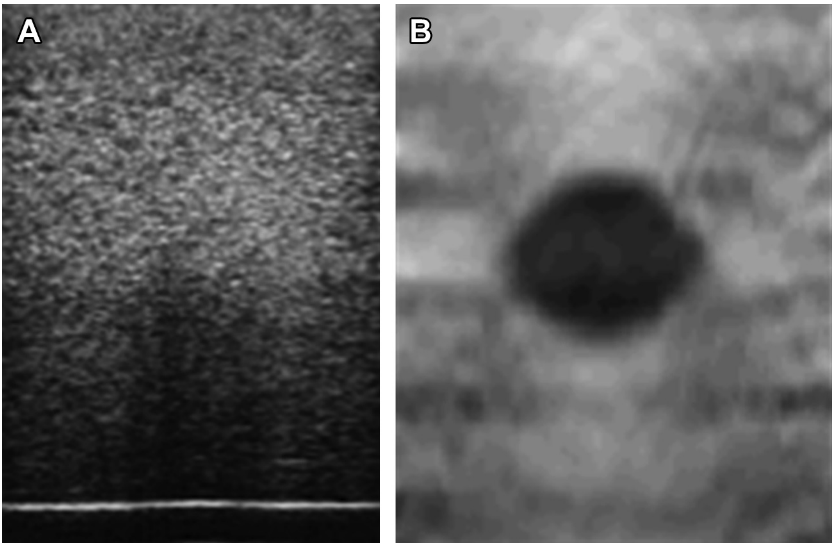

Fig. 2. Sonogram (*A*) and strain (*B*) elastograms obtained from a phantom containing a single 10-mm diameter inclusion whose modulus contrast was approximately 6.03 dB.

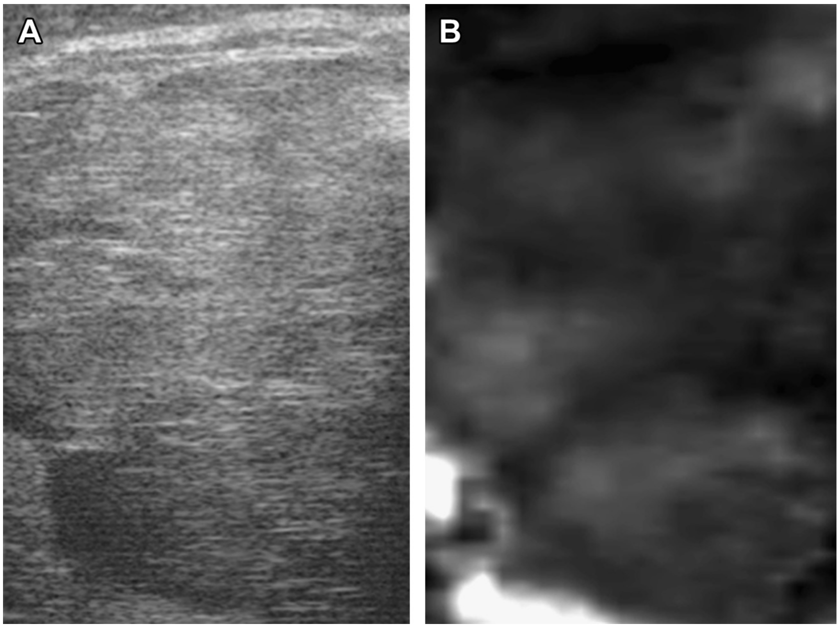

Fig. 3. Sonographic (*A*) and elastographic (*B*) images of phyllodes breast tumor. (*Courtesy of* Dr Jeff Bamber, Institute of Cancer Research in London, London, England.)

In the sonogram shown in **Fig. 3**, the tumor covers most of the field of view, with the capsule of the anterior margin visible close to the top of the image and the posterior margin visible at the bottom left. Within the tumor, the appearance is heterogeneous on a large scale, with macroscopic lobules separated by echogenic boundaries that are probably fibrous in nature. The strain elastogram (see **Fig. 3**B) confirms this appearance but shows it much more clearly with greater contrast than the sonogram (see **Fig. 3**A). The macroscopic lobules within the tumor are clearly defined as soft regions separated by stiff septa, which is consistent with the septa being of a fibrous nature.

Direct and iterative inversion schemes have been developed to make quasistatic elastograms more quantitative. These techniques compute

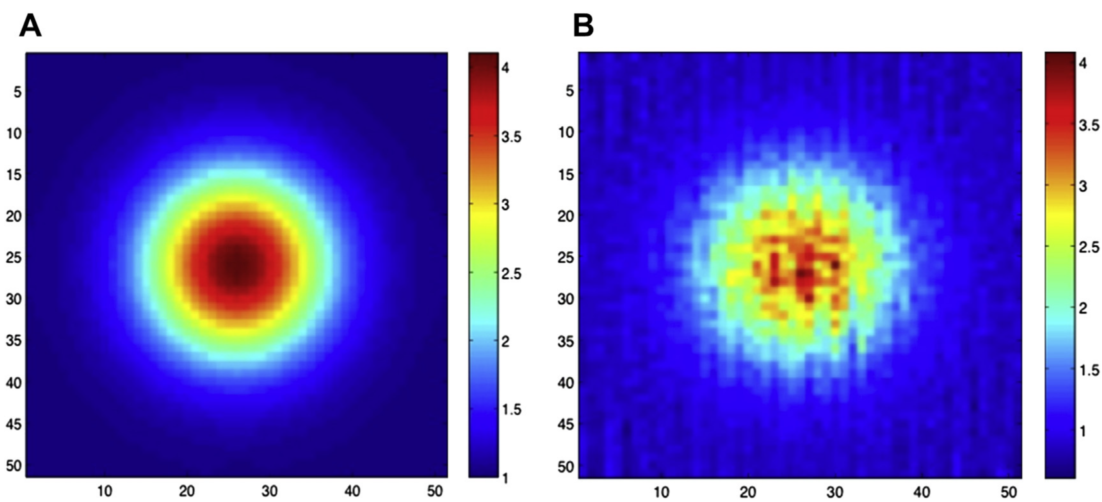

Fig. 4. Modulus elastograms computed from ideal axial and lateral strain estimates (*A, left*) and (*B, right*) strain estimates that were corrupted with 4% additive white noise. The simulated phantom contained an inclusion with a gaussian modulus distribution that had a peak contrast of 4:1. (*Courtesy of* Dr P. Barbone, Boston University Department of Mechanical and Aeronautic Engineering, Boston, MA.)

the Young's or shear modulus from the measured displacement or strain using the forward elasticity model described in Equation 7. Direct inversion schemes use a linear system of equations derived by rearranging the PDEs that describe the forward elastography problem.[8,28,39]

$$(\partial_{yy} - \partial_{xx})(\varepsilon_{xy}\mu) + \partial_{xy}(\varepsilon_{xy}\mu) = 0 \tag{14}$$

Equation 14 contains high-order derivatives that amplify measurement noise, which compromises the quality of ensuing modulus elastograms, as demonstrated in **Fig. 4**.

Iterative inversion techniques[40,41] overcome this issue by considering the inverse problem as a parameter-optimization task, where the goal is to find the Young's modulus that minimizes the error between measured displacement or strain fields and those computed by solving the forward elastography problem. The matrix solution at the (k + 1) iteration that has the general form:

$$\mu^{k+1} = \Delta\mu^k + \left[J(\mu^k)^T J(\mu^k) + \rho I\right]^{-1} J(\mu^k)^T (u_m - u\{\mu^k\}) \tag{15}$$

where $\Delta\mu^k$ is a vector of shear modulus updates at all coordinates in the reconstruction field and J is the Jacobian, or sensitivity, matrix. The Hessian matrix, $[J(\mu^k)^T J(\mu^k)]$, is ill conditioned. Therefore, to stabilize performance in the presence of measurement noise, the matrix is regularized using 1 of 3 variational methods: the Tikhonov,[41] the Marquardt,[42] or the total variational method.[43,44] **Fig. 5** shows an example of modulus elastograms computed with the iterative inversion approach.

The contrast-to-noise ratio of the modulus elastogram is better than that of the strain elastogram, which improved the detection of the boundary between the ablated region and normal tissue to enable accurate determination of the size of the thermal zone.

Harmonic Elastography Based on Local Frequency Estimation

In harmonic elastography,[5,5–9,34,45] low-frequency acoustic waves (typically <1 kHz) are transmitted within the tissue using a sinusoidal mechanical source. The phase and amplitude of the propagating waves are visualized using either color Doppler imaging[34,45,46] (**Fig. 6**) or phase-contrast MRI.[9–11]

Assuming that shear waves propagate with plane wave fronts, then an approximate estimate of the local shear modulus (μ) may be computed from local estimates of the wavelength:

$$v_{shear} = \sqrt{\frac{\mu}{\rho}} \tag{16}$$

where v_{shear} is the velocity of the shear wave, and ρ is the density of the tissue. In a homogeneous tissue, shear modulus can be estimated from local estimates of instantaneous frequency.[47,48] Although shear modulus estimated using this approach is insensitive to measurement noise, the spatial resolution of the ensuing modulus elastograms is limited. A further weakness of the approach is that the plane wave approximation breaks down in complex organs, such as the breast and brain, when waves reflected from internal tissue boundaries interfere constructively and destructively.

Like quasistatic elastography, solving the inverse elastography problem improves the performance of harmonic elastography. **Fig. 7** shows a representative example of an elastogram obtained from a healthy volunteer by solving the inverse harmonic elastography problem. The resolution of the elastograms was sufficiently high to visualize fibroglandular tissue from the adipose tissue.[49,50]

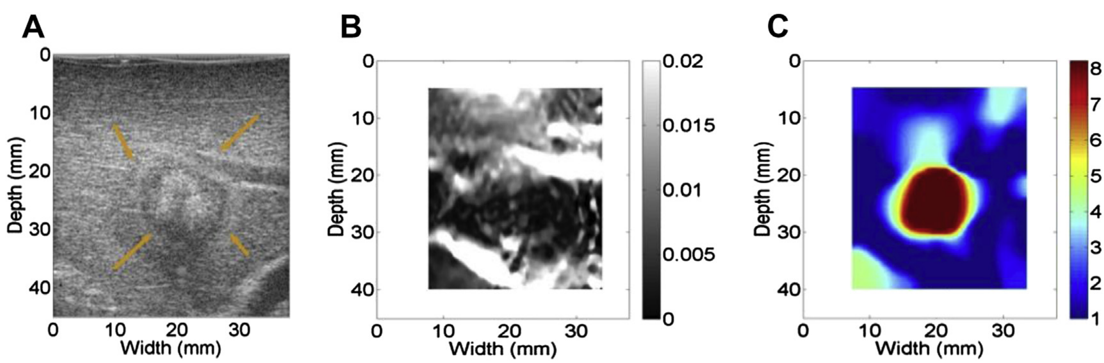

Fig. 5. Sonogram with arrows indicating ablated tissue (*A*), strain elastogram (*B*), and modulus elastogram (*C*) of RF ex vivo ablated bovine liver. (*Courtesy of* Drs T.J. Hall, T. Varghese, and J. Jiang, University of Wisconsin-Madison, Madison, WI.)

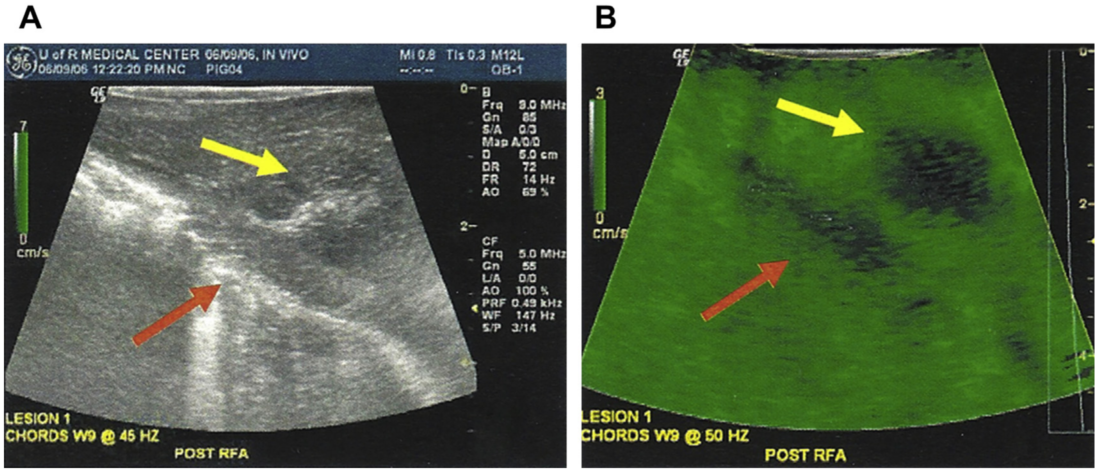

Fig. 6. In vivo porcine liver with a thermal lesion. The sonogram (*A*) shows a lesion with indistinct boundaries. The sonoelastogram (*B*) demonstrates a vibration deficit indicating a hard lesion. Yellow arrows point to the lesion. Red arrows point the boundary of the liver.

Transient Elastography Based on Arrival Time Estimation

A major limitation of harmonic elastography is that shear waves attenuate rapidly as they propagate within soft tissues, which limits the depth of penetration. The transient approach to elastography overcomes this limitation by using the acoustic radiation force of an ultrasound transducer to perturb tissue locally.[51–53] This elastographic imaging method uses an ultrasound scanner with an ultrahigh frame rate (ie, 10,000 frames per second) to track the propagation of shear waves. As in harmonic elastography, local estimates of shear modulus are estimated from local estimates of wavelength. The reflections of shear waves at internal tissue boundaries make it difficult, however, to measure shear wave velocity—this limitation can be overcome by computing wave speeds directly from the arrival times, as discussed by Ji

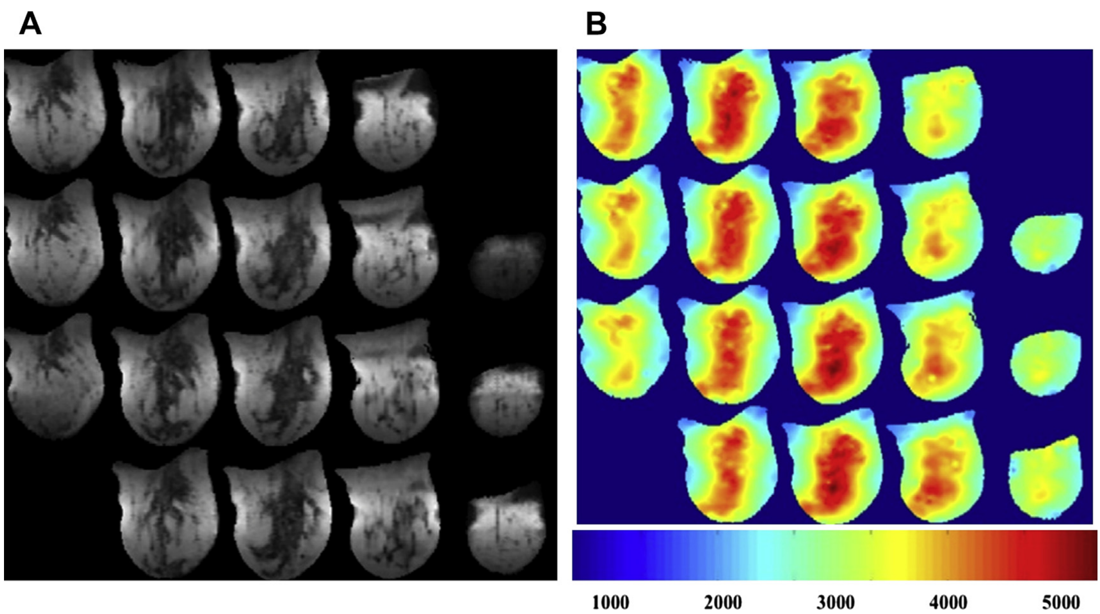

Fig. 7. Montage of magnitude MRIs (*A*) and shear modulus elastograms (*B*) recovered from a healthy volunteer using the subzone inversion scheme. (*Courtesy of* Drs J.B. Weaver and K.D. Paulsen, Dartmouth College, Thayer School of Engineering, Dartmouth, NH.)

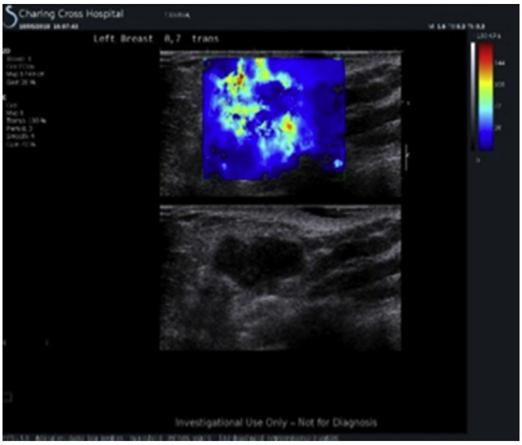

Fig. 8. Comparison transient shear wave (*upper*) and B-scan (*lower*) images of a breast with pathology confirmed IDC. The maximum diameter on the longitudinal axis on B-mode was 17 mm, whereas both elastographic techniques indicated a larger footprint of the cancer. (*Courtesy of* Dr W. Svensson, Imperial College, London).

and colleagues.[54] **Fig. 8** shows an example of shear wave elastograms obtained from a breast cancer patient using a commercially available transient elastography system.

THE FUTURE OF ELASTOGRAPHY

Soft tissues display several biomechanical properties, including viscosity and nonlinearity, which may improve the diagnostic value of elastography when visualized alone or in combination with shear modulus. For example, clinicians could use mechanical nonlinearity to differentiate between benign and malignant breast tumors.[1] Furthermore, there is mounting evidence that other mechanical parameters, namely viscosity[55,56] and anisotropy,[57] could also differentiate between benign and malignant tissues—similar claims have also been made for shear modulus.[57] Not only can these mechanical parameters discriminate between different tissue types but also they may provide value in other clinical areas, including brain imaging,[58,59] distinguishing the mechanical properties of active and passive muscle groups,[60–62] characterizing blood clots,[63] and gnosing edema.[64] Several investigators are actively developing techniques to visualize different mechanical properties using quasistatic, harmonic, and transient elastographic imaging approaches.

Viscoelasticity

In most approaches to elastography, the mechanical behavior of soft tissues is modeled using the theory of linear elasticity (Hooke's law), which is an appropriate model for linear elastic materials (ie, Hookean materials). It is well known, however, that most materials, including soft tissues, deviate from Hooke's law in various ways. Materials that exhibit both fluid-like and elastic (ie, viscoelastic) mechanical behavior deviate from Hooke's law.[20] For viscoelastic materials, the relationship between stress and strain is dependent on time. Viscoelastic materials display 3 unique mechanical behaviors: (1) strain increases with time when stress (externally applied load) is sustained over a period of time, a phenomenon known as viscoelastic creep; (2) stress decreases with time when strain is held constant, a phenomenon known as viscoelastic relaxation; and (3) during cyclic loading, mechanical energy is dissipated in the form of heat, a phenomenon known as hysteresis.

Several investigators are actively developing elastographic imaging methods to visualize the mechanical parameters that characterize linear viscoelastic materials (ie, viscosity, shear modulus, and Poisson ratio). For example, Asbach and colleagues[60] developed a multifrequency method to measure the viscoelastic properties of normal liver tissue versus diseased liver tissue taken from patients with grades 3 and 4 liver fibrosis. They computed the shear modulus and viscosity variations within the tissue by fitting a Maxwell rheological model to the measured data and solving the linear viscoelastic wave equation in the frequency domain. They observed that fibrotic liver tissue had a higher viscosity (14.4 ± 6.6 Pa s) and elastic modulus ($\mu_1 = 2.91 \pm 0.84$ kPa and $\mu_2 = 4.83 \pm 1.77$ kPa) than normal liver tissue. Their results revealed that although liver tissue is dispersive, it appeared as nondispersive between the frequency range of 25 Hz to 50 Hz. Catheline and colleagues[65] computed the shear modulus (μ) and viscosity (η) by fitting the measured speed of sound and attenuation equation to Voigt and Maxwell rheological models. They observed that the recovered shear modulus values were independent of the rheological model used, but viscosity values were highly dependent on the models used.

Sinkus and colleagues[56] developed a direct-inversion scheme to visualize the mechanical properties of visocelastic materials, in which a curl operation was performed on the time-harmonic displacement field $\mathbf{u}(\mathbf{x},t) = \mathbf{u}(\mathbf{x},t)e^{i\omega t}$ to remove the displacement contribution of the compressional wave. They derived the governing equation that describes the motion incurred in an isotropic, viscoelastic medium by computing the curl of the PDEs that describe the motion incurred by both transverse and compressional shear waves. The resulting PDEs for transverse waves are given in compact form by:

$$\rho\partial_t^2\mathbf{u} = \mu\nabla^2\mathbf{u} + \eta\partial_t\nabla^2\mathbf{u} \quad \mathbf{(17)}$$

Sinkus and colleagues[56] developed a direct-inversion scheme from Equation 17, in which μ and η were the unknowns. They evaluated the inversion scheme using (1) computer simulations, (2) phantom studies, and (3) patient studies. Their simulation studies revealed that the proposed algorithm could accurately recover shear modulus and viscosity from ideal displacement data. With noisy displacements, however, a good estimate of shear modulus was obtained only when the shear modulus of the simulated tissue was less than 8 kPa. The inversion scheme overestimated the shear modulus values when actual stiffness of the tissue was larger than 8 kPa. A similar effect was observed when estimating viscosity, albeit much earlier (ie, the algorithm provided good estimates of viscosity when μ <5 kPa). Although the shear modulus affected the bias in the viscosity measurement, the investigators demonstrated that the converse did not occur (ie, the viscosity did not affect the bias in shear modulus). Despite these issues, their phantom studies revealed that inclusions were discernible in both μ and η elastograms, and the viscosity values agreed with previously reported values for gelatin (0.21 Pa s). The patient studies revealed that the shear modulus values of malignant breast tumors were noticeably higher than those of benign fibroadenomas, but there was no significant difference observed in the viscosity of the tumor types, a result that seems to contradict results reported by Qiu and colleagues.[55]

Nonlinearity

When soft tissues deform by a small amount (an infinitesimal deformation), their geometry in the undeformed and deformed states is similar, thus the deformation is characterized using engineering strain. To characterize finite deformation, first a reference configuration has to be defined, which is the geometry of the tissue under investigation in either the deformed or undeformed state. The Green-Lagrangian strain is defined as:

$$\varepsilon_{ij} = \frac{1}{2}\left[\frac{\partial u_i}{\partial x_j} + \frac{\partial u_j}{\partial x_i} + \frac{\partial u_k}{\partial x_i}\frac{\partial u_k}{\partial x_j}\right] \quad \mathbf{(18)}$$

The nonlinear term is neglected when the magnitude of the spatial derivative is small, to produce the linear strain tensor, as defined in Equation 4. The relationship between stress and strain is nonlinear even for a linearly elastic material when it is undergoing finite deformations. Consequently, Skovoroda and colleagues[66] proposed a direct-inversion scheme to reconstruct the shear modulus distribution of a linear elastic material that is undergoing finite deformation.

Some materials exhibit nonlinear material properties that are typically described using a strain energy density function. Among the strain energy functions proposed in the literature, the most widely used for modeling tissues are (1) the neo-Hookean hyperelastic model and (2) the neo-Hookean model with an exponential term. Oberai and colleagues[67] used a different model, the Veronda-Westman strain energy density function (W), to describe the finite displacement of a hyperelastic solid that is undergoing finite deformation, which is defined by:

$$W = \mu_0\left(\frac{e^{\gamma(I_1-3)} - 1}{\gamma} - \frac{I_2 - 3}{2}\right) \quad \mathbf{(19)}$$

where the terms I_1 and I_2 are the first and second invariants of the Cauchy-Green strain tensor, μ_0 is the shear modulus, and γ denotes the nonlinearity. For the nonlinear case, they proposed an iterative inversion approach to reconstruct a nonlinear parameter and the shear modulus at zero strain.

Using data obtained from volunteer breast cancer patients, one with a benign fibroadenoma tumor and another with an invasive ductal carcinoma (IDC), Oberai and colleagues[67] observed that for the fibroadenoma case, the tumor was visible in modulus elastograms that had been computed using small strain and large strain (12%), although the contrast of the elastograms computed at large strain (7:1) was lower than that computed at smaller strain (10:1). The fibroadenoma tumor was not visible in nonlinear parameter elastograms. The inclusion in the patient with IDC was discernible in shear modulus elastograms recovered using small and large strains. The stiffness contrast of the modulus elastograms recovered at both small and large strains was comparable, however, and the IDC tumor was visible in nonlinear parameter elastograms. This result is one of several that have demonstrated the clinical value of nonlinear elastographic imaging. Specifically, elastography can characterize the nonlinear behavior of soft tissues and may be used to differentiate between benign and malignant tumors.

REFERENCES

1. Krouskop TA, Wheeler TM, Kallel F, et al. Elastic moduli of breast and prostate tissues under compression. Ultrason Imaging 1998;20:260–74.

2. Parker KJ, Doyley MM, Rubens DJ. Imaging the elastic properties of tissue: the 20 year perspective. Phys Med Biol 2011;56:R1–29.
3. Samani A, Zubovits J, Plewes D. Elastic moduli of normal and pathological human breast tissues: an inversion-technique-based investigation of 169 samples. Phys Med Biol 2007;52:1565–76.
4. Sarvazyan AP, Skovoroda AR, Emelianov SY, et al. Biophysical bases of elasticity imaging. Acoust Imaging 1995;21:223–40.
5. Lerner RM, Parker KJ, Holen J, et al. Sono-elasticity: medical elasticity images derived from ultrasound signals in mechanically vibrated targets. Acoust Imaging 1988;16:317–27.
6. O'Donnell M, Skovoroda AR, Shapo BM, et al. Internal displacement and strain imaging using ultrasonic speckle tracking. IEEE Trans Ultrason Ferroelectrics Freq Contr 1994;41(3):314–25.
7. Ophir J, Cespedes I, Ponnekanti H, et al. Elastography: a quantitative method for imaging the elasticity of biological tissues. Ultrason Imaging 1991;13:111–34.
8. Bishop J, Samani A, Sciarretta J, et al. Two-dimensional MR elastography with linear inversion reconstruction: methodology and noise analysis. Phys Med Biol 2000;45:2081–91.
9. Muthupillai R, Lomas DJ, Rossman PJ, et al. Magnetic-resonance elastography by direct visualization of propagating acoustic strain waves. Science 1995;269:1854–7.
10. Sinkus R, Lorenzen J, Schrader D, et al. High-resolution tensor MR elastography for breast tumour detection. Phys Med Biol 2000;45:1649–64.
11. Weaver JB, Van Houten EE, Miga MI, et al. Magnetic resonance elastography using 3D gradient echo measurements of steady-state motion. Med Phys 2001;28:1620–8.
12. Khalil AS, Chan RC, Chau AH, et al. Tissue elasticity estimation with optical coherence elastography: toward mechanical characterization of In vivo soft tissue. Ann Biomed Eng 2005;33:1631–9.
13. Kirkpatrick SJ, Wang RK, Duncan DD. OCT-based elastography for large and small deformations. Opt Express 2006;14:11585–97.
14. Ko HJ, Tan W, Stack R, et al. Optical coherence elastography of engineered and developing tissue. Tissue Eng 2006;12:63–73.
15. Bamber JC, Barbone PE, Bush NL, et al. Progress in freehand elastography of the breast. IEICE Trans Inf Sys 2002;E85d:5–14.
16. Greenleaf JF, Fatemi M, Insana M. Selected methods for imaging elastic properties of biological tissues. Annu Rev Biomed Eng 2003;5:57–78.
17. Manduca A, Dutt V, Borup DT, et al. Inverse approach to the calculation of elasticity maps for magnetic resonance elastography. SPIE Med Imaging Proceedings 1998;3338:426–36.
18. Ophir J, Garra B, Kallel F, et al. Elastographic imaging. Ultrasound Med Biol 2000;26(Suppl 1):S23–9.
19. Doyley MM. Model-based elastography: a survey of approaches to the inverse elasticity problem. Phys Med Biol 2012;57:R35–73.
20. Fung YC. Biomechanics: mechanical properties of living tissue. New York: Springer; 1981.
21. Timoshenko SP, Goodier JN. Theory of elasticity. Singapore: McGraw-Hill; 1970.
22. Landau LD, Lifshitz EM, Kosevich AM, et al. Theory of elasticity. Oxford (United Kingdom): Elsevier Butterworth-Heinemann; 1986.
23. Ophir J, Alam SK, Garra B, et al. Elastography: ultrasonic estimation and imaging of the elastic properties of tissues. Proc Inst Mech Eng H 1999;213:203–33.
24. Van Houten EE, Miga MI, Weaver JB, et al. Three-dimensional subzone-based reconstruction algorithm for MR elastography. Magn Reson Med 2001;45:827–37.
25. Bilgen M, Insana M. Elastostatics of a spherical inclusion in homogeneous biological media. Phys Med Biol 1998;43:1–20.
26. Kallel F, Bertrand M, Ophir J. Fundamental limitations on the contrast-transfer efficiency in elastography: an analytic study. Ultrasound Med Biol 1996;22:463–70.
27. Love A. The stress produced in a semi-infinite solid by pressure on part of the boundary. In: Philosophical transactions of the Royal Society of London, vol 228. London: The Royal Society; 1929. p. 377–420.
28. Sumi C, Suzuki A, Nakayama K. Estimation of shear modulus distribution in soft-tissue from strain distribution. IEEE Trans Biomed Eng 1995;42:193–202.
29. Brigham JC, Aquino W, Mitri FG, et al. Inverse estimation of viscoelastic material properties for solids immersed in fluids using vibroacoustic techniques. J Appl Phys 2007;101:023509–1–14.
30. Hall TJ, Bilgen M, Insana MF, et al. Phantom materials for elastography. IEEE Trans Ultrason Ferroelectrics Freq Contr 1997;44:1355–65.
31. Konofagou E, Dutta P, Ophir J, et al. Reduction of stress nonuniformities by apodization of compressor displacement in elastography. Ultrasound Med Biol 1996;22:1229–36.
32. McLaughlin J, Renzi D. Shear wave speed recovery in transient elastography and supersonic imaging using propagating fronts. Inverse Probl 2006;22:681–706.
33. Miga MI. A new approach to elastography using mutual information and finite elements. Phys Med Biol 2003;48:467–80.
34. Parker KJ, Huang SR, Musulin RA, et al. Tissue-response to mechanical vibrations for sonoelasticity imaging. Ultrasound Med Biol 1990;16:241–6.

35. Ponnekanti H, Ophir J, Cespedes I. Ultrasonic-imaging of the stress-distribution in elastic media due to an external compressor. Ultrasound Med Biol 1994;20:27–33.
36. Samani A, Bishop J, Plewes DB. A constrained modulus reconstruction technique for breast cancer assessment. IEEE Trans Med Imaging 2001; 20:877–85.
37. Bamber JC, Bush NL. Freehand elasticity imaging using speckle decorrelation rate. New York: Plenum Press; 1995.
38. Rizzatto G, Chersevani R, Solbiati L. High resolution ultrasound assists in breast diagnosis. Diagn Imaging Int 1993;9:42–5.
39. Skovoroda AR, Aglyamov SR. On reconstruction of elastic properties of soft biological tissues exposed to low-frequencies. Biofizika 1995;40:1329–34.
40. Doyley MM, Bamber JC, Shiina T, et al. Reconstruction of elasticity modulus distribution from envelope detected B-mode data. Proc IEEE Ultrason Symp 1996;2:1611–4.
41. Kallel F, Bertrand M. Tissue elasticity reconstruction using linear perturbation method. IEEE Trans Med Imaging 1996;15:299–313.
42. Doyley MM, Meaney PM, Bamber JC. Evaluation of an iterative reconstruction method for quantitative elastography. Phys Med Biol 2000;45:1521–40.
43. Jiang J, Varghese T, Brace CL, et al. Young's modulus reconstruction for radio-frequency ablation electrode-induced displacement fields: a feasibility study. IEEE Trans Med Imaging 2009; 28:1325–34.
44. Richards MS, Barbone PE, Oberai AA. Quantitative three-dimensional elasticity imaging from quasi-static deformation: a phantom study. Phys Med Biol 2009;54:757–79.
45. Yamakoshi Y, Sato J, Sato T. Ultrasonic imaging of internal vibrtation of soft tissue under forced vibration. IEEE Trans Ultrason Ferroelectrics Freq Contr 1990;37:45–53.
46. Lerner RM, Huang SR, Parker KJ. "Sonoelasticity" images derived from ultrasound signals in mechanically vibrated tissues. Ultrasound Med Biol 1990; 16:231–9.
47. Manduca A, Oliphant TE, Dresner MA, et al. Magnetic resonance elastography: non-invasive mapping of tissue elasticity. Med Image Anal 2001;5: 237–54.
48. Wu Z, Hoyt K, Rubens DJ, et al. Sonoelastographic imaging of interference patterns for estimation of shear velocity distribution in biomaterials. J Acoust Soc Am 2006;120:535–45.
49. Doyley MM, Srinivasan S, Pendergrass SA, et al. Compartive evaluation of strain-based and model-based modulus elastography. Ultrasound Med Biol 2004;31:787–802.
50. Van Houten EE, Doyley MM, Kennedy FE, et al. Initial in vivo experience with steady-state subzone-based MR elastography of the human breast. J Magn Reson Imaging 2003;17:72–85.
51. McAleavey S, Collins E, Kelly J, et al. Validation of SMURF estimation of shear modulus in hydrogels. Ultrason Imaging 2009;31:131–50.
52. Nightingale K, McAleavey S, Trahey G. Shear-wave generation using acoustic radiation force: in vivo and ex vivo results. Ultrasound Med Biol 2003;29: 1715–23.
53. Sarvazyan AP, Rudenko OV, Swanson SD, et al. Shear wave elasticity imaging: a new ultrasonic technology of medical diagnostics. Ultrasound Med Biol 1998;24:1419–35.
54. Ji L, McLaughlin JR, Renzi D, et al. Interior elastodynamics inverse problems: shear wave speed reconstruction in transient elastography. Inverse Probl 2003;19:S1–29.
55. Qiu YP, Sridhar M, Tsou JK, et al. Ultrasonic viscoelasticity imaging of nonpalpable breast tumors: preliminary results. Acad Radiol 2008;15: 1526–33.
56. Sinkus R, Tanter M, Xydeas T, et al. Viscoelastic shear properties of in vivo breast lesions measured by MR elastography. Magn Reson Imaging 2005; 23:159–65.
57. Sinkus R, Tanter M, Catheline S, et al. Imaging anisotropic and viscous properties of breast tissue by magnetic resonance-elastography. Magn Reson Med 2005;53:372–87.
58. Hamhaber U, Klatt D, Papazoglou S, et al. In vivo magnetic resonance elastography of human brain at 7 T and 1.5 T. J Magn Reson Imaging 2010;32: 577–83.
59. Sack I, Beierbach B, Wuerfel J, et al. The impact of aging and gender on brain viscoelasticity. Neuroimage 2009;46:652–7.
60. Asbach P, Klatt D, Hamhaber U, et al. Assessment of liver viscoelasticity using multifrequency MR elastography. Magn Reson Med 2008;60: 373–9.
61. Hoyt K, Castaneda B, Parker KJ. Two-dimensional sonoelastographic shear velocity imaging. Ultrasound Med Biol 2008;34:276–88.
62. Perrinez PR, Kennedy FE, Van Houten EE, et al. Modeling of soft poroelastic tissue in time-harmonic MR elastography. IEEE Trans Biomed Eng 2009;56:598–608.
63. Schmitt C, Soulez G, Maurice RL, et al. Noninvasive vascular elastography: toward a complementary characterization tool of atherosclerosis in carotid arteries. Ultrasound Med Biol 2007;33: 1841–58.
64. Righetti R, Garra BS, Mobbs LM, et al. The feasibility of using poroelastographic techniques for

distinguishing between normal and lymphedematous tissues in vivo. Phys Med Biol 2007;52: 6525–41.

65. Catheline S, Gennisson J, Delon G, et al. Measurement of viscoelastic properties of homogeneous soft solid using transient elastography: an inverse problem approach. J Acoust Soc Am 2004;116: 3734–41.

66. Skovoroda AR, Lubinski MA, Emelianov SY, et al. Reconstructive elasticity imaging for large deformations. IEEE Trans Ultrason Ferroelectrics Freq Contr 1999;46:523–35.

67. Oberai AA, Gokhale NH, Goenezen S, et al. Linear and nonlinear elasticity imaging of soft tissue in vivo: demonstration of feasibility. Phys Med Biol 2009;54:1191–207.